Supplement of Atmos. Chem. Phys., 21, 973–987, 2021
https://doi.org/10.5194/acp-21-973-2021-supplement

Atmospheric Chemistry and Physics
Open Access
EGU

Supplement of

Measurement report: quantifying source contribution of fossil fuels and biomass-burning black carbon aerosol in the southeastern margin of the Tibetan Plateau

Huikun Liu et al.

Correspondence to: Qiyuan Wang (wangqy@ieecas.cn) and Junji Cao (cao@loess.llqg.ac.cn)

Text S1. Chemical composition measurements

S1.1 Water-soluble ion analysis

The concentrations of K^+ were determined with the use of a Dionex DX-600 ion chromatograph (IC, Dionex Inc., Sunnyvale, CA, USA) equipped with IonPac CS12A column (20m Methane sulfonic acid as the eluent) for cation analysis. Quality assurance/quality control (QA/QC) procedures were based on the analysis of standard reference materials produced by the National Research Center for Certified Reference Materials in China. To extract the water-soluble ions from the quartz filters, one quarter of each weighed filter was placed in a 15 mL vial containing 10 mL distilled deionized water (18.2 MΩ resistivity). The vials were placed in an ultrasonic water bath and shaken with a mechanical shaker for 1 h to extract the ions. The extracts were filtered through 0.45 μm pore-size microporous membranes, and the filtrates were stored at 4 °C in clean tubes before instrumental analysis.

S1.2 OC/EC analysis

Elemental carbon (EC) and organic carbon (OC) were measured with the use of a DRI Model 2001 Thermal/Optical Carbon Analyzer (Atmoslytic Inc., Calabasas, CA, USA) and a thermal/optical reflectance (TOR) method. The IMPROVE_A protocol was used for the analysis. A punch aliquot of a quartz filter sample was heated in a stepwise manner to obtain data for four OC fractions (OC1, OC2, OC3, and OC4) in a helium atmosphere at 140°C, 280°C, 480°C, 580°C, and three EC fractions (EC1, EC2, and EC3) in a 2% oxygen, 98% helium atmosphere at 580°C, 740°C, 840°C. Pyrolyzed carbon (OP) was produced at < 580°C in the inert atmosphere: this component decreases the reflected light and is used to correct for charred OC. Total OC is defined as the sum of the four OC fractions plus OP, and total EC is the sum of the three EC fractions minus OP. The QA/QC procedures for these analyses have been described in detail in Cao et al., (2003).

S1.3 Elemental analysis

Elements including S, Ca, Ti, Mn, Fe, Cu, As, Br, Pb and Zn were quantified by energy-dispersive X-ray fluorescence (ED-XRF) spectrometry (Epsilon 5 ED-XRF, PANalytical B.V., Netherlands). The ED-XRF instrument used a three-dimensional polarizing geometry with eleven secondary targets and one barkla target. Good signal to background ratios and low detection limits are achieved for the method. The X-ray source was a side window X-ray tube with a gadolinium anode, and it operated at an accelerating voltage of 25e100 kV and a current of 0.5e24 mA (maximum power: 600 W). The characteristic X-ray radiation was detected by a germanium detector (PANalytical 32). Each sample was analysed for ~30 min to obtain a spectrum of X-ray counts versus photon energies, with the individual peak energies matching specific elements, and peak areas corresponding to elemental concentrations. The ED-XRF spectrometer was calibrated with thin-film standards obtained from MicroMatter Co. (Arlington, WA, USA).

S1.4 Levoglucosan analysis

The filter samples were extracted in 15 mL vials that each contained 10 mL of distilled deionized water (18.2 MΩ resistivity). The extractions were done in an ultrasonic water bath where the tubes were mechanically shaken for 15 mins and repeated for 4 times with 30 mins interval; then 0.45-mm pore size microporous membranes were used to filter out insoluble materials. High-performance anion exchange chromatography with a Dionex DX-600 ion chromatograph (Dionex Inc., Sunnyvale, CA, USA) equipped with a pulsed amperometric detector (HPAEC-PAD) was used to quantify levoglucosan. Levoglucosan was separated by a Dionex CarboPac MA1 analytical column (4 x 250 mm) and a Dionex CarboPac MA1 guard column with sodium hydroxide solution (612 mM) as eluent at the flow rate of 0.4 mL min^{-1}. The analyses required 1 hr for each sample. The method detection limit (MDL, signal/noise = 3/1) of levoglucosan was 1.3 ng mL^{-1}.

S1.5 Benzothiazolone analysis

Filter samples were extracted with 5mL of methanol in 20 mL vials, the volumes of the extracts were adjusted to 5ml using rotary evaporator with the target analytes in it. Aliquots of 50μL of the extracts were adjusted to pH 9.1 with 50 μL of a borate buffer. Later, the filter samples were subject to ultrasound-assisted extraction for 20 min. The final extracts were then diluted with a 3:1 mixture of water and acetone. The mixture also included 40 μL dansyl chloride and 10 μL of an internal standard solution. After 1 min of agitation in a vortex shaker, the reaction mixture was subject to ultrasound irradiation for 15 min at 35°C, and afterwards, the reaction vials were stored in the dark. The derivatized products were analysed with a high performance liquid chromatograph (HPLC, Series 1200; Agilent Technology) furnished with a Waters Sunfire C18 column (2.1 × 150 mm, 3.5-μm particle size) coupled to an ion-trap mass spectrometer (Esquire 3000; Bruker Daltonics, Billerica, MA, USA). The minimum detection limit of benzothiazolone was 0.0153 ng cm^{-2}. Replicate analysis of standards demonstrated that the precision of the analysis was < 6.9%.

Table S1 OPAC modeled b_{scat} (M m^{-1}), b_{abs} (M m^{-1}), SSA and PAX measured b_{scat} (M m^{-1}), b_{abs} (M m^{-1}), SSA

Date	PAX b_{abs}(532)	OPAC b_{abs}(550)	b_{abs} difference	PAX b_{scat}(532)	OPAC b_{scat}(550)	b_{scat} difference	SSA PAX	SSA OPAC	SSA difference
2018/3/15	7.47	7.23	-3.24%	61.33	60.20	-1.85%	0.89	0.89	0.07%
2018/3/16	5.82	5.81	-0.25%	62.71	61.40	-2.08%	0.92	0.91	-0.11%
2018/3/17	3.48	3.62	3.96%	84.30	84.30	0.00%	0.96	0.96	-0.14%
2018/3/18	3.75	3.78	0.70%	46.12	44.40	-3.73%	0.92	0.92	-0.30%
2018/3/19	2.60	2.70	3.69%	19.84	20.20	1.82%	0.88	0.88	-0.34%
2018/3/20	3.01	3.02	0.25%	24.98	25.30	1.29%	0.89	0.89	0.18%
2018/3/21	2.62	2.69	2.58%	29.93	30.10	0.58%	0.92	0.92	-0.16%
2018/3/22	8.63	8.53	-1.20%	88.01	89.60	1.81%	0.91	0.91	0.26%
2018/3/23	10.30	10.04	-2.51%	94.02	96.10	2.21%	0.90	0.91	0.41%
2018/3/24	7.85	7.80	-0.69%	76.08	78.30	2.91%	0.91	0.91	0.06%
2018/3/25	7.54	7.74	2.66%	67.48	69.20	2.55%	0.90	0.90	0.06%
2018/3/27	9.46	9.48	0.26%	85.27	86.70	1.68%	0.91	0.90	-0.91%
2018/3/28	2.49	2.50	0.44%	39.34	39.42	0.20%	0.94	0.94	-0.27%
2018/3/29	4.14	4.04	-2.33%	53.20	54.49	2.42%	0.93	0.93	0.34%

2018/3/30	5.92	5.95	0.58%	76.74	77.07	0.43%	0.93	0.93	-0.01%
2018/3/31	4.06	3.98	-1.97%	40.34	39.36	-2.44%	0.91	0.91	-0.06%
2018/4/1	3.32	3.26	-1.72%	35.03	35.14	0.31%	0.91	0.92	0.16%
2018/4/3	3.51	3.50	-0.42%	35.66	35.82	0.44%	0.91	0.91	0.03%
2018/4/4	6.62	6.58	-0.70%	54.47	54.70	0.43%	0.89	0.89	0.05%
2018/4/5	6.55	6.61	0.87%	56.55	55.90	-1.15%	0.90	0.89	-0.20%
2018/4/6	3.07	3.08	0.18%	37.79	37.46	-0.88%	0.92	0.92	-0.09%
2018/4/7	1.51	1.50	-0.34%	14.59	14.70	0.72%	0.91	0.91	0.08%
2018/4/8	4.36	4.42	1.39%	72.50	71.22	-1.77%	0.94	0.94	-0.14%
2018/4/9	2.74	2.78	1.29%	31.25	31.20	-0.18%	0.92	0.92	-0.14%
2018/4/10	2.29	2.27	-0.70%	25.70	25.65	-0.20%	0.92	0.92	-0.04%
2018/4/11	1.88	1.85	-1.48%	23.86	23.45	-1.71%	0.93	0.93	-0.01%
2018/4/12	3.24	3.16	-2.36%	32.51	32.85	1.04%	0.91	0.91	-0.07%
2018/4/13	17.51	17.20	-1.76%	41.31	41.80	1.19%	0.70	0.71	0.81%
2018/4/14	4.37	4.40	0.61%	20.81	20.22	-2.83%	0.83	0.82	-0.61%
2018/4/15	0.75	0.76	1.76%	15.77	15.77	0.02%	0.95	0.95	-0.08%
2018/4/16	2.20	2.21	0.52%	28.55	28.73	0.64%	0.93	0.93	-0.05%

2018/4/17	4.75	4.77	0.54%	43.22	43.09	-0.30%	0.90	0.90	-0.12%
2018/4/18	6.76	6.80	0.54%	81.87	81.27	-0.73%	0.92	0.92	-0.10%
2018/4/19	3.06	3.05	-0.34%	66.41	66.53	0.18%	0.96	0.96	0.01%
2018/4/20	2.36	2.4	1.62%	25.87	25.87	-0.02%	0.92	0.91	-0.45%
2018/4/21	3.34	3.35	0.27%	46.69	46.72	0.07%	0.93	0.93	-0.03%
2018/4/22	3.14	3.09	-1.57%	45.00	45.75	1.66%	0.93	0.94	0.13%
2018/4/23	2.61	2.68	2.76%	25.13	25.54	1.62%	0.91	0.91	0.25%
2018/4/24	3.93	3.88	-1.38%	36.72	36.68	-0.10%	0.90	0.90	0.12%
2018/4/25	5.52	5.54	0.43%	48.44	48.59	0.31%	0.90	0.90	-0.03%
2018/4/26	10.49	10.42	-0.70%	89.62	90.06	0.49%	0.90	0.89	-0.18%
2018/4/27	7.44	7.20	-3.35%	73.20	73.77	0.78%	0.91	0.91	0.37%
2018/4/28	7.74	7.66	-1.05%	77.17	77.59	0.54%	0.91	0.91	0.17%
2018/4/29	5.76	5.85	1.50%	57.98	57.47	-0.87%	0.91	0.91	-0.22%
2018/4/30	3.93	4.03	2.53%	85.00	85.40	0.47%	0.96	0.96	-0.09%
2018/5/1	4.92	4.97	0.99%	62.85	63.23	0.60%	0.93	0.93	-0.02%
2018/5/2	4.42	4.42	-0.08%	71.81	71.42	-0.55%	0.94	0.94	-0.11%
2018/5/3	2.72	2.75	1.23%	54.48	54.01	-0.87%	0.95	0.95	-0.10%

2018/5/4	2.26	2.29	1.18%	47.52	47.46	-0.12%	0.95	0.95	-0.05%
2018/5/5	0.45	0.45	0.86%	15.19	15.14	-0.35%	0.97	0.97	-0.03%
2018/5/6	0.90	0.93	3.01%	22.21	21.60	-2.74%	0.96	0.96	-0.41%
2018/5/7	1.56	1.54	-1.20%	21.75	21.77	0.08%	0.93	0.93	0.09%
2018/5/8	1.27	1.28	0.53%	26.74	26.36	-1.41%	0.95	0.95	-0.09%
2018/5/9	1.77	1.71	-3.33%	23.71	23.90	0.82%	0.93	0.93	0.30%
2018/5/10	1.20	1.22	1.49%	13.55	13.57	0.13%	0.92	0.92	-0.10%
2018/5/11	1.37	1.36	-0.53%	14.47	14.23	-1.66%	0.91	0.91	-0.10%

Abbreviations: OPAC Optical Properties of Aerosols and Clouds, PAX Photoacoustic Extinctiometer; b_{scat} aerosol light scattering coefficient; b_{abs} aerosol light absorption coefficient; SSA single scattering albedo.

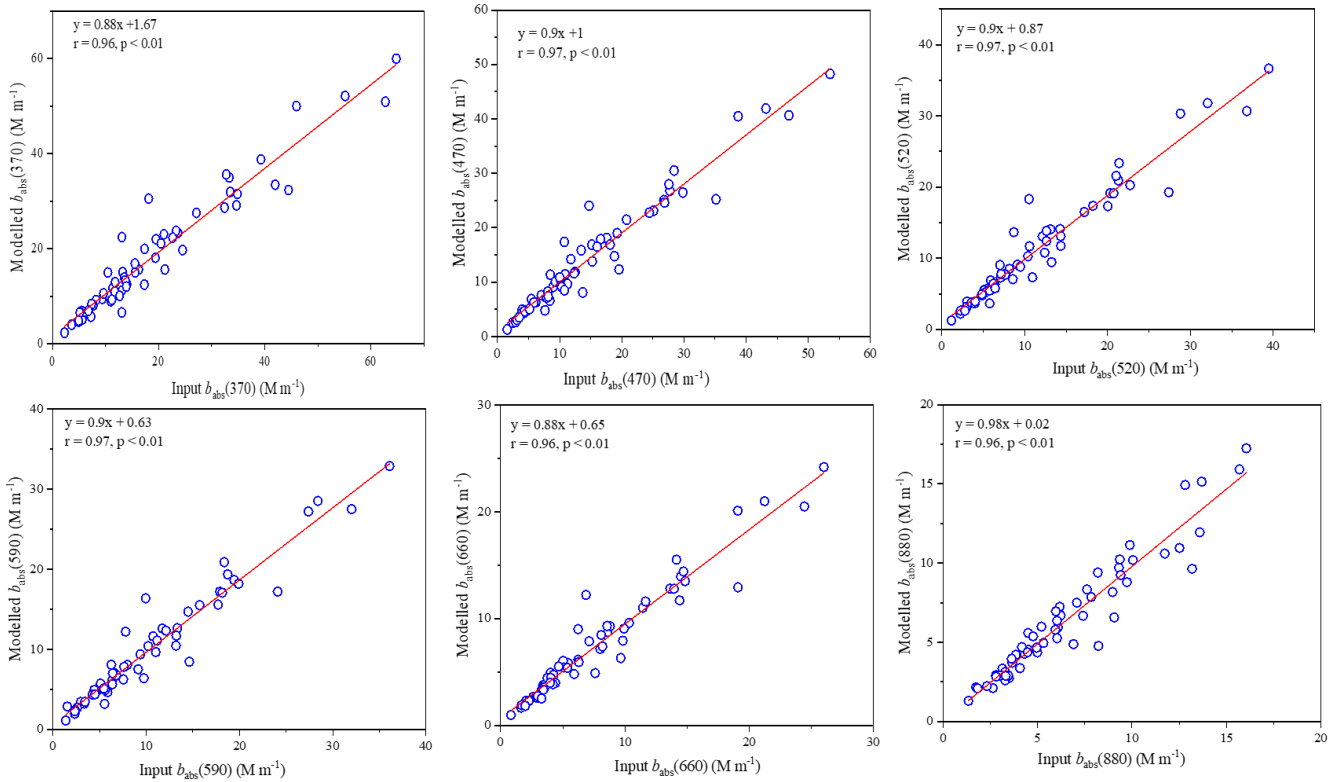

Figure S1. Correlations between the modeled primary aerosol light absorption coefficient $b_{abs}(\lambda)$ obtained from the positive matrix factorization model and the input values estimated using the black carbon-tracer method. λ represents wavelengths of 370, 470, 520, 590, 660, or 880 nm.

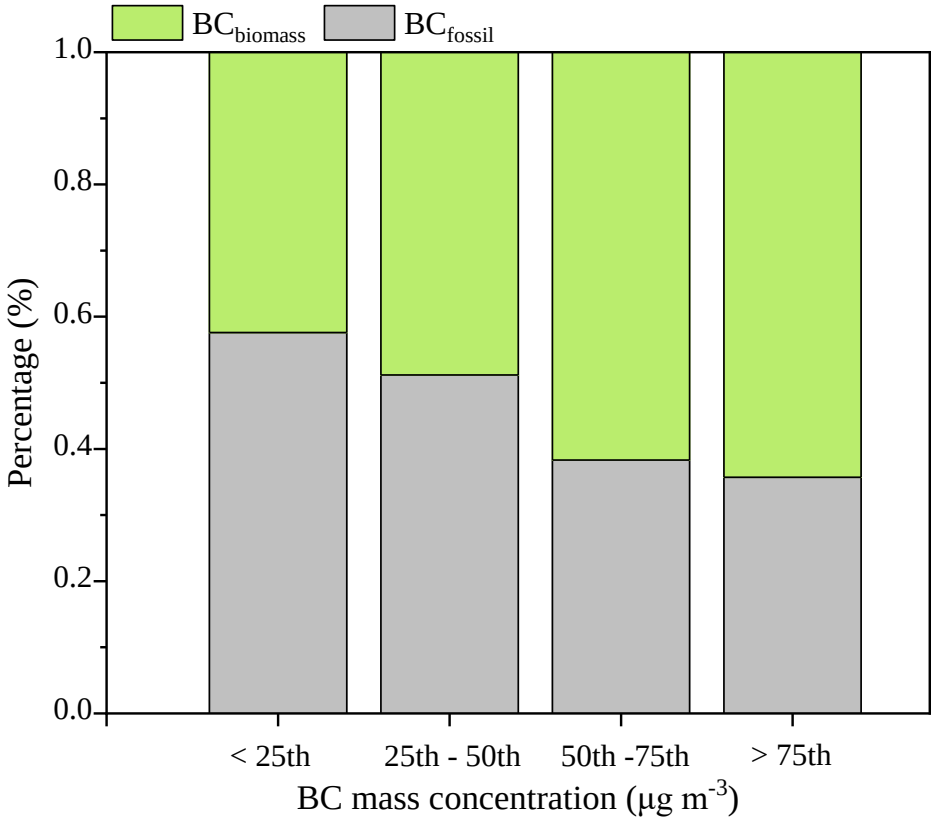

Figure S2. Mass percentages of total black carbon (BC) mass by quartile from biomass burning ($BC_{biomass}$) and fossil fuel combustion (BC_{fossil}).

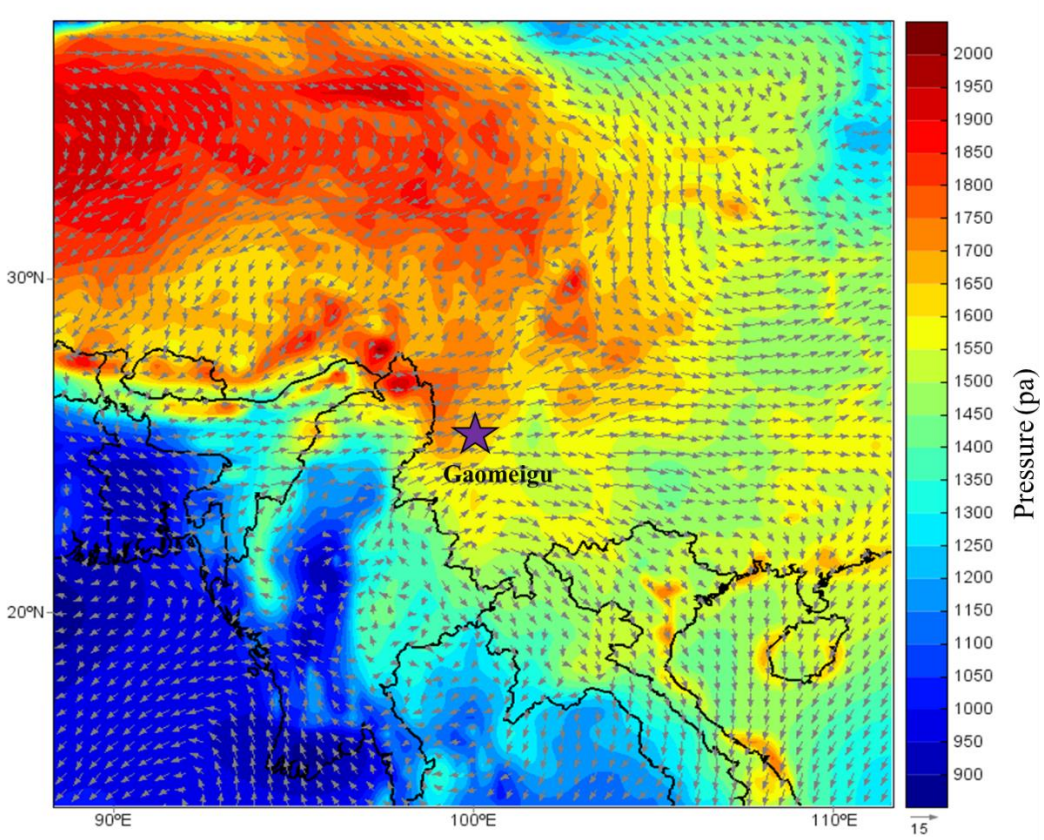

Figure S3. Spatial distributions of wind direction, wind speed (m s^{-1}) and barometric pressure (Pa) in the morning (8 am to 12 am). The purple star represents the sampling site.

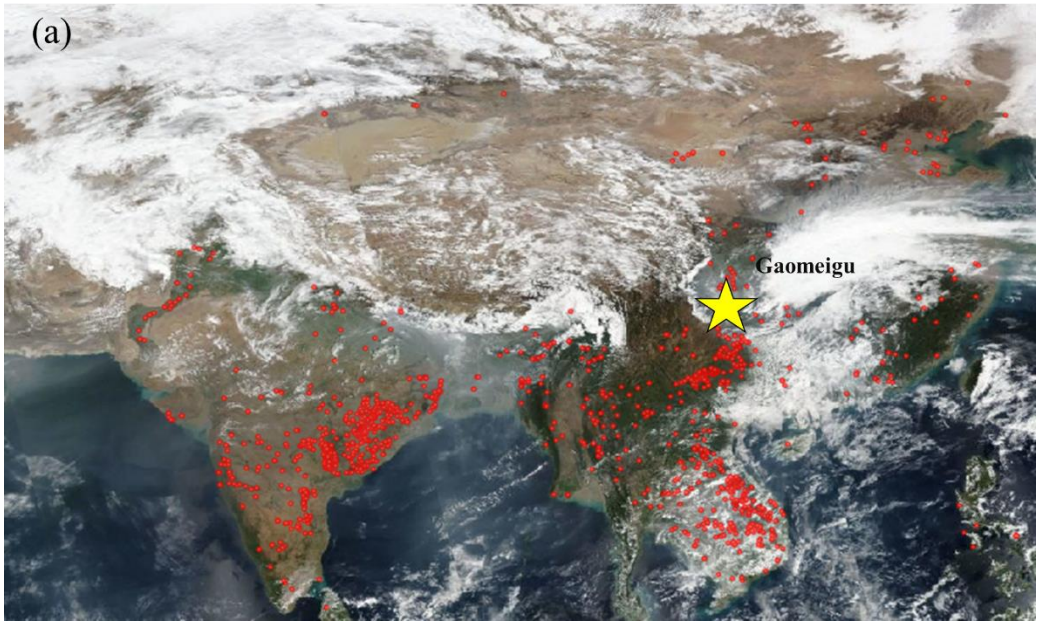
(a)
Gaomeigu

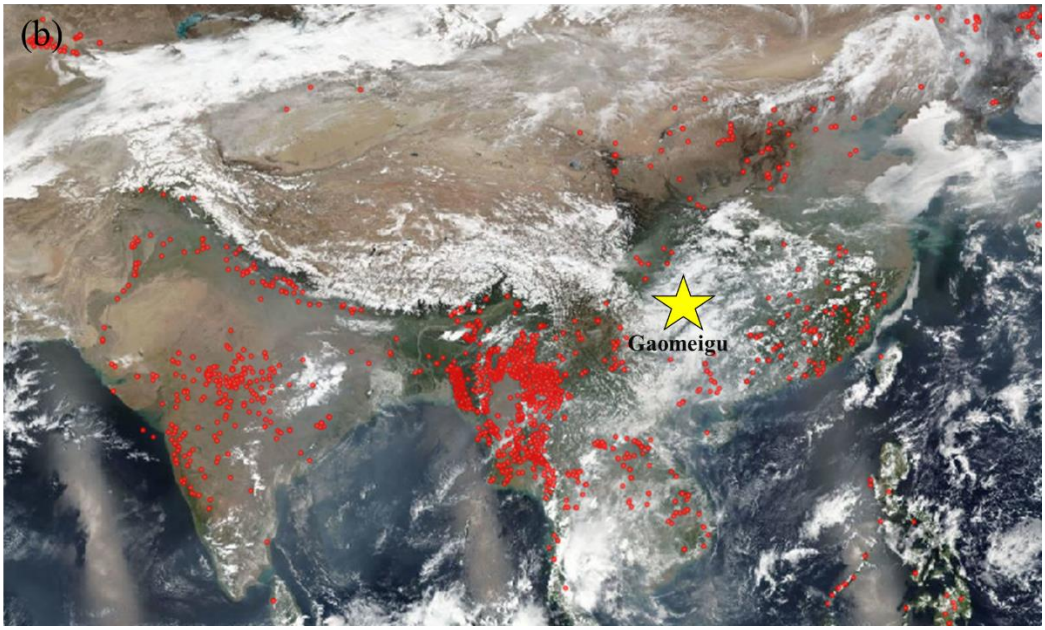
(b)
Gaomeigu

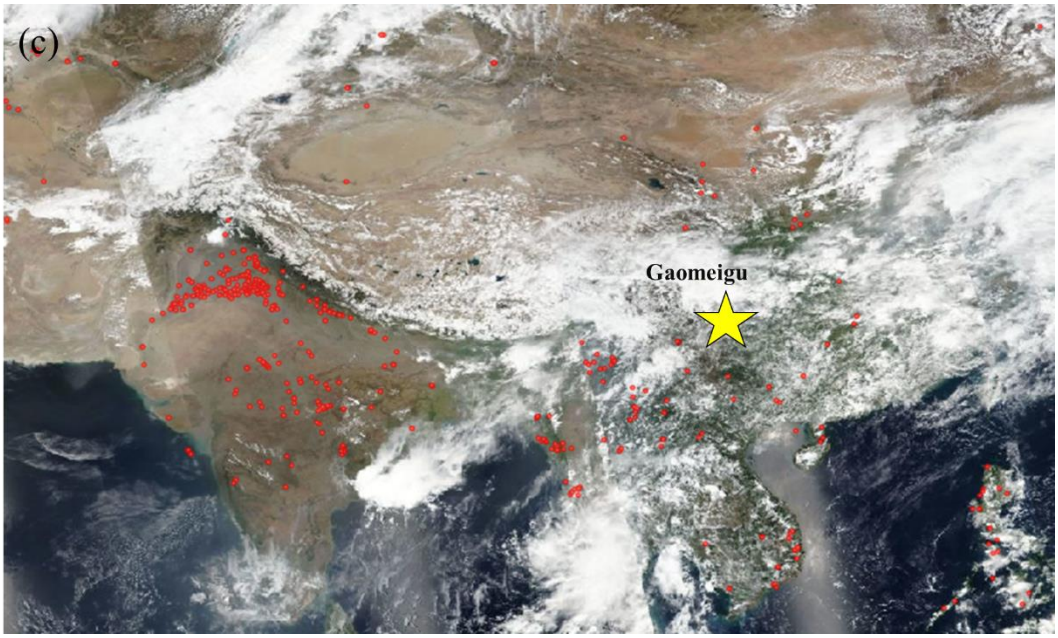

Figure S4. Monthly average fire site maps for (a) March 2018, (b) April 2018, and (c) May 2018. The fire site maps are from © NASA (National Aeronautics and Space Administration) (https://www.nasa.gov/image-feature/goddard/2018/a-world-on-fire)

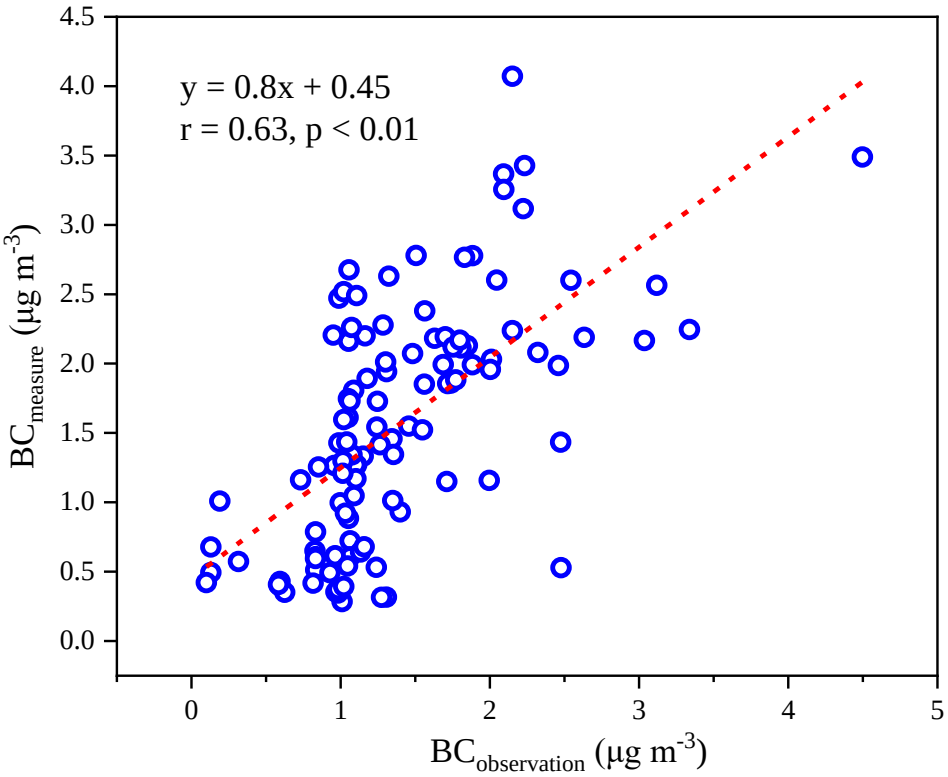

Figure S5. Scatter plot of the measured black carbon (BC) mass concentrations versus those obtained from the Weather Research and Forecasting model.

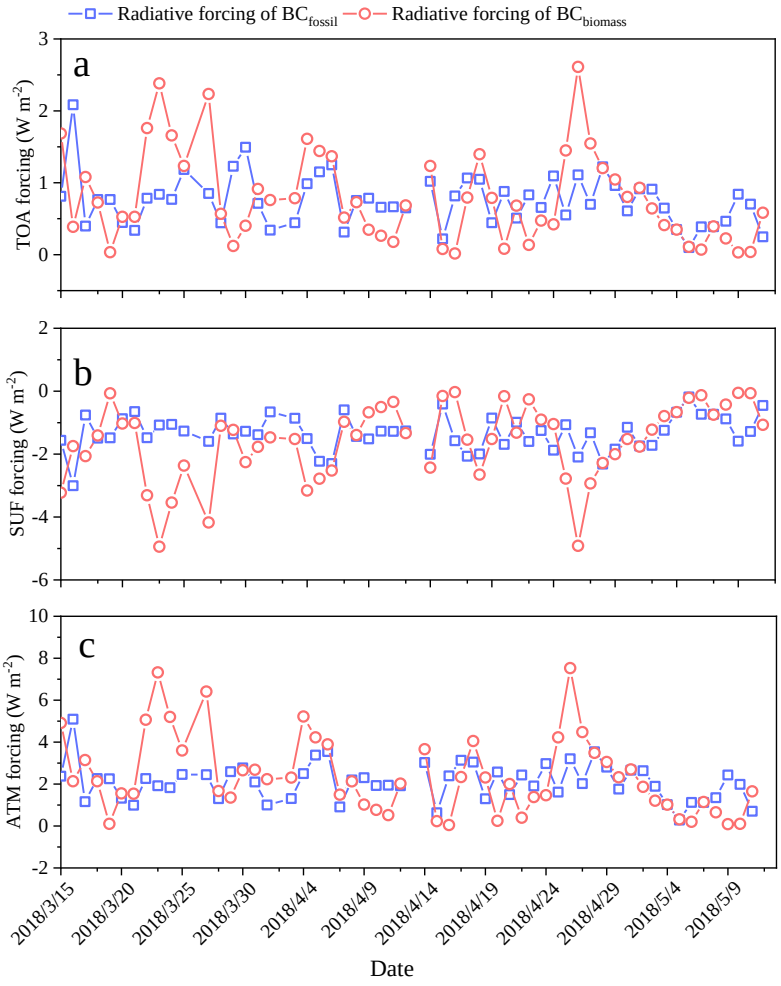

Figure S6. (a) Daily radiative effects of black carbon (BC) from biomass burning ($BC_{biomass}$) and BC from fossil fuel combustion (BC_{fossil}) at the top of atmosphere (TOA), (b) at the surface (SUF), and (c) in the atmosphere (ATM).

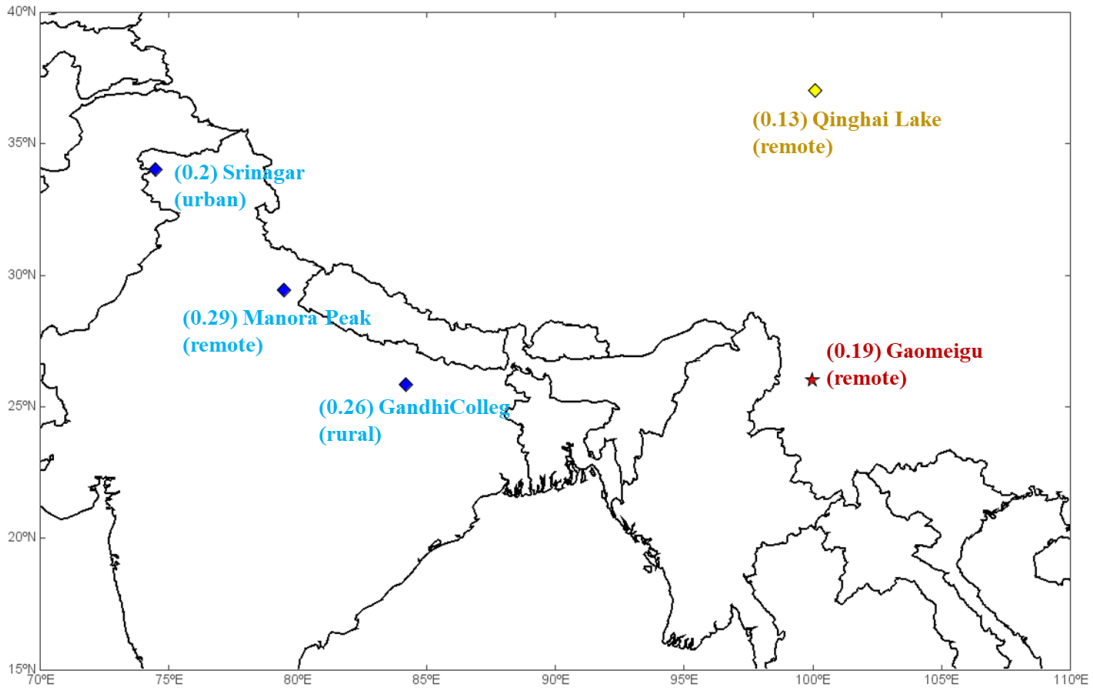

Figure S7. Heating rates calculated from black carbon (BC) concentrations (units are (K day^{-1}) ($\mu g\ m^{-3}$)$^{-1}$) for the Himalayas and the Tibetan Plateau reported in previous studies (Srivastava et al., 2012; Tiwari et al., 2016; Bhat et al., 2017; Wang et al., 2015).

References

Bhat, M. A., Romshoo, S. A., and Beig, G.: Aerosol black carbon at an urban site-Srinagar, Northwestern Himalaya, India: Seasonality, sources, meteorology and radiative forcing, Atmos. Environ., 165, 336-348, 10.1016/j.atmosenv.2017.07.004, 2017.

Cao, J. J., Lee, S. C., Ho, K. F., Zhang, X. Y., Zou, S. C., Fung, K., Chow, J. C., and Watson, J. G.: Characteristics of carbonaceous aerosol in Pearl River Delta Region, China during 2001 winter period, Atmos. Environ., 37, 1451-1460, 10.1016/S1352-2310(02)01002-6, 2003.

Srivastava, A. K., Ram, K., Pant, P., Hegde, P., and Joshi, H.: Black carbon aerosols over Manora Peak in the Indian Himalayan foothills: implications for climate forcing, Environmental Research Letters, 7, 10.1088/1748-9326/7/1/014002, 2012.

Tiwari, S., Dumka, U. C., Hopke, P. K., Tunved, P., Srivastava, A. K., Bisht, D. S., and Chakrabarty, R. K.: Atmospheric heating due to black carbon aerosol during the summer monsoon period over Ballia: A rural environment over Indo-Gangetic Plain, Atmospheric Research, 178-179, 393-400, 10.1016/j.atmosres.2016.04.008, 2016.

Wang, Q. Y., Huang, R. J., Cao, J. J., Tie, X. X., Ni, H. Y., Zhou, Y. Q., Han, Y. M., Hu, T. F., Zhu, C. S., Feng, T., Li, N., and Li, J. D.: Black carbon aerosol in winter northeastern Qinghai–Tibetan Plateau, China: the source, mixing state and optical property, Atmos. Chem. Phys., 15, 13059-13069, 10.5194/acp-15-13059-2015, 2015.